Absorption heat pump cycles with NH_3 – ionic liquid working pairs

Wang, Meng; Infante Ferreira, Carlos A.

DOI
10.1016/j.apenergy.2017.07.074

Publication date
2017

Document Version
Final published version

Published in
Applied Energy

Applied Energy 204 (2017) 819–830

Contents lists available at ScienceDirect

Applied Energy

journal homepage: www.elsevier.com/locate/apenergy

Absorption heat pump cycles with NH_3 – ionic liquid working pairs

Meng Wang*, Carlos A. Infante Ferreira

Process and Energy Department, Delft University of Technology, Leeghwaterstraat 39, 2628 CB Delft, The Netherlands

HIGHLIGHTS

- Nine NH_3/IL pairs are investigated in AHPs for building heating.
- COP of four NH_3/IL pairs beats that of the NH_3/H_2O.
- Idealized NH_3/IL mixture can reach a COP of 1.84.
- [Emim][SCN] is currently a feasible candidate to be used in AHPs with PHX.

ARTICLE INFO

Keywords:
Absorption cycle
Heat pump
NH_3
ILs
Optimization
Economic analysis

ABSTRACT

Ionic liquids (ILs), as novel absorbents, draw considerable attention for their potential roles in replacing water or LiBr aqueous solutions in conventional NH_3/H_2O or H_2O/LiBr absorption refrigeration or heat pump cycles. In this paper, performances of 9 currently investigated NH_3/ILs pairs are calculated and compared in terms of their applications in the single-effect absorption heat pumps (AHPs) for the floor heating of buildings. Among them, 4 pairs were reported for the first time in absorption cycles (including one which cannot operate for this specific heat pump application). The highest coefficient of performance (COP) was found for the working pair using [mmim][DMP] (1.79), and pairs with [emim][Tf_2N] (1.74), [emim][SCN] (1.73) and [bmim][BF_4] (1.70) also had better performances than that of the NH_3/H_2O pair (1.61). Furthermore, an optimization was conducted to investigate the performance of an ideal NH_3/IL pair. The COP of the optimized mixture could reach 1.84. Discussions on the contributions of the generator heat and optimization results revealed some factors that could affect the performance. It could be concluded that the ideal IL candidates should show high absorption capabilities, large solubility difference between inlet and outlet of the generator, low molecular weights and low heat capacities. In addition, an economic analysis of the AHP using NH_3/[emim][SCN] working pair with plate heat exchangers was carried out based on heat transfer calculations. The results indicated that the NH_3/IL AHP is economically feasible. The efforts of heat transfer optimization in the solution heat exchanger and a low expense of ILs can help the IL-based AHP systems to become more promising.

1. Introduction

The Paris Agreement adopted by 195 countries in the 2015 Paris climate conference (COP 21) reset the global ambition: limiting the temperature rise from pre-industrial levels well below 2 K. Efforts responding to climate change are also accelerating the way the energy sector is developing [1]. Heating and cooling, especially for buildings take up the majority of the energy consumption and the greenhouse gases emission. According to the European Commission, heating and cooling consumed 50% (22.85 EJ) of the final energy consumption in the EU in 2012. 45% of energy for heating and cooling in the EU was used in the residential sector, 37% in industry and 18% in services [2]. In the US, 41% (42.2 EJ) of the primary energy in 2010 was consumed by the buildings sector, compared to 30% by the industrial sector and 29% by the transportation sector. Heating and cooling took 59% of the buildings energy consumption [3]. As an increasingly significant energy consumer in the buildings sector, China is the largest energy-consuming economy in the world, and buildings energy used in China was the second-largest in the world after the US, representing nearly 16% of total global energy consumption in buildings in 2012 (more than 18 EJ) [4].

Absorption refrigeration and heat pump cycles are drawing considerable attention because they can take effective advantage of low-grade heat from concentrating solar collectors or waste heat, providing opportunities for clean and sustainable energy utilizations [5–8]. Working pairs H_2O/LiBr and NH_3/H_2O have been widely used in

* Corresponding author.
E-mail address: M.Wang-2@tudelft.nl (M. Wang).

http://dx.doi.org/10.1016/j.apenergy.2017.07.074
Received 19 December 2016; Received in revised form 17 July 2017; Accepted 18 July 2017

Nomenclature

A	area (m^2)
C	cost (k€)
C_p	heat capacity (kJ kg^{-1} K^{-1}/kJ $kmol^{-1}$ K^{-1})
c	coefficient in heat capacity (–)
f	circulation ratio (–)
G	parameters in NRTL model (–)
h	specific enthalpy (kJ kg^{-1})
$\dot{m}$	mass flow rate (kg s^{-1})
Mw	molecular weight (kg $kmol^{-1}$)
P	pressure (Pa)
Q	heat flow (W)
q	quality (kg kg^{-1})
T	temperature (K/°C)
w	mass concentration (kg kg^{-1})
x	molar concentration (kmol $kmol^{-1}$)

Greek letter

α	parameter in NRTL model (–)
γ	activity coefficient (–)
τ	parameter in NRTL model (–)

Subscript and superscript

0	reference state
1,2 …	state point
abs	absorber
c	critical (property)
con	condenser
E	excess (enthalpy)
eva	evaporator
gen	generator
NH_3	species of NH_3
IL	species of IL
phx	plate heat exchanger
r	refrigerant stream
s	strong solution stream
sat	saturated state
sol	solution
sthx	shell-and-tube heat exchanger
vap	vapor

Abbreviation

ABS	absorber
AHP	absorption heat pump
CON	condenser
COP	coefficient of performance
EOS	equation of state
EVA	evaporator
GA	genetic algorithm
GAX	generator/absorber heat exchanger
GEN	generator
HC	hydrocarbon
HFC	hydrochlorofluorocarbon
HX	heat exchangers
IL	ionic liquid
NRTL	non-random two-liquid activity coefficient model
OHTC	overall heat transfer coefficient
PHX	plate heat exchanger
REC	rectifier
RMSD	root-mean-square deviation
RK	Redlich-Kwong (equation of state)
SHX	solution heat exchanger
VLE	vapor-liquid equilibrium/vapor-liquid equilibria
[mmim][DMP]	1,3-dimethylimidazolium dimethyl phosphate
[emim][BF_4]	1-ethyl-3-methylimidazolium tetrafluoroborate
[hmim][BF_4]	1-hexyl-3-methylimidazolium tetrafluoroborate
[omim][BF_4]	1-methyl-3-octylimidazolium tetrafluoroborate
[bmim][BF_4]	1-butyl-3-methylimidazolium tetrafluoroborate
[bmim][PF_6]	1-butyl-3-methylimidazolium hexafluorophosphate
[emim][Tf_2N]	1-ethyl-3-methylimidazolium bis(trifluoromethylsulfonyl) imide
[emim][$EtSO_4$]	1-ethyl-3-methylimidazolium ethylsulfate
[emim][SCN]	1-ethyl-3-methylimidazolium thiocyanate

certain applications in absorption systems, while many challenges do exist, such as crystallization possibilities of the H_2O/LiBr pair and the difficulty in the separation of the NH_3/H_2O pair [9]. Thus, the investigation of alternative solvents is still a relevant topic [10–14,9].

Ionic liquids (ILs), whose properties can be adjusted by the design of anion and cation combination for a task-specified purpose, have drawn considerable attention for their potential roles in replacing conventional absorbents used in absorption refrigeration and heat pump cycles in the past years. Researchers recognized the strengths of ILs in applications, such as high boiling point, good affinity with refrigerants, and high chemical and thermal stabilities [9]. Nevertheless, there are also some challenges related to the technical feasibility and costs when introducing them, thus many efforts are still needed before the ILs are accepted in practice.

In order to preselect promising ILs to be used in absorption systems, many researchers did performance investigations. The majority of investigations were focused on performance predictions, in which the frequently studied refrigerants include H_2O [15,16], hydrocarbons (HCs) [17], hydrofluorocarbons (HFC) [18,19] and CO_2 [20]. Since NH_3 based absorption systems hold strengths such as sub-zero degree applications and free of air infiltration, research related to these mixtures is most relevant. Nevertheless, there is only limited work which has been reported. Yokozeki and Shiflett [21,22] measured solubility data for NH_3 with a set of ILs, and calculated the thermodynamic performance of these mixtures in a single-effect cycle. Kotenko [23] also developed thermodynamic simulations for absorption heat pumps (AHPs) with 4 NH_3/ILs mixtures in Aspen Plus, and compared their performances with that of the NH_3/H_2O system. Their results showed that the efficiency of some of the investigated NH_3/IL AHP processes, at specified operating conditions, was higher than that of conventional NH_3/H_2O systems. Chen et al. [24,25] investigated vapor-liquid equilibria (VLE) for metal ion-containing ionic liquid [bmim][Zn_2Cl_5] with NH_3, and compared the thermodynamic performance of this mixture with that of the NH_3/NaSCN pair. The performance of the former system is better than that of the latter one when the generator temperature is high and the absorber and the condenser temperatures are low. Ruiz et al. [26] modeled NH_3/IL absorption using COSMO-based Aspen simulations and analyzed cycle performance for conventional and task-specific ILs.

In these performance prediction studies of absorption systems, the enthalpy of the NH_3/IL solution is always an essential thermodynamic property. Most researchers obtained this property by adding an excess enthalpy to the sum of enthalpies of the two pure components. The excess enthalpy could be obtained from the VLE data via a variety of models. Some researchers [27,15,28] used the non-random two-liquid (NRTL) activity coefficient model to predict it. However, Shiflett and Yokozeki [27] found that an accurate prediction of the mixing enthalpy with NRTL is very difficult, because the excess enthalpy is derived from

the temperature derivative of the activity coefficient, and the temperature-dependency in any activity model is always in a purely empirical form. Therefore then they turned to a cubic equation of state (EOS) method for excess enthalpy predictions [21,22]. Meanwhile, for the pure components part, one of the challenges is the heat capacity of the IL. In the work of Yokozeki and Shiflett [21,22], this part was obtained from a group function contribution method [29]. However, Cai et al. [20] pointed out that this group function contribution method is not always accurate. In the prediction work of Chen et al. [25], experimental heat capacity data of ILs were employed in the enthalpy predictions. Therefore, according to the previous studies, the combination of EOS based method for the excess enthalpy with the experimental heat capacity data of ILs may provide a more accurate way for the performance prediction of AHPs.

Previous experimental studies were carried out either by substituting the working pairs in a traditional commercial system [30–32] with H_2O/ILs pairs, or restricted to small scales systems [33]. Apart from these studies, the understanding of ILs in more practical aspects, for example the heat and mass transfer aspects, is still limited. However, researches of IL-based working pairs is emerging recently taking more practical aspects into account. Meyer et al. [34] studied the combined heat and mass transfer phenomena of H_2O/[emim][DEP] pairs in an absorption refrigeration system by using analytical functions. Ariyadi and Coronas [35] developed a measurement setup to study the absorption capacity of the NH_3 vapor in ILs in a pool type absorber. Wadekar [36] simulated the heat transfer behavior of IL [bmim][Tf_2N] in different heat exchangers (HXs). The results showed that the heat transfer performance was not particularly attractive, but heat transfer enhancement technology can improve it effectively. Boman et al. [37] screened working pairs including the IL-based ones for a single-effect AHP based on both thermodynamic and heat transfer principles. The shell-and-tube HXs of IL-based AHP systems need more heat exchanger area due to the poor heat transfer performance of the ILs. Chugh et al. [38] implemented a membrane-based semi-open absorption system using IL for heating, dehumidification and cooling application. The experimental test achieved a heating coefficient of performance (COP) of 1.4.

In this paper, a thermodynamic model of single-effect AHPs is first proposed accompanied with an accurate method to estimate enthalpies of solutions. With this model, the performance behaviors of 9 commercialized ILs with NH_3 are investigated along with that of the conventional NH_3/H_2O pair. Considering previous studies, the 9 working pairs cover all the ILs which have sufficient published data (VLE data with NH_3 and pure heat capacities of ILs) for this calculation. The performance of four of these pairs in absorption systems is reported for the first time. The influence of the GEN temperatures on the circulation ratio (f) and on the COP is also studied. As one of the most original parts of this study, the developed NRTL and heat capacity models have been made generic, by integrating them with a genetic algorithm (GA) in the thermodynamic AHP model, to determine the maximum COP of the AHP cycle and explore how the thermodynamic properties of the ideal ILs should show. In addition, the heat transfer calculations for each heat exchanger of an AHP are carried out considering all heat exchangers are plate heat exchangers (PHXs). Based on that, the feasibility of applying IL in an AHP system is analyzed by investigating its economic performance.

2. Methods

2.1. Thermodynamic model of the cycle

Thermodynamic models of the single-effect AHP systems have been frequently reported in the literature, see for instance Kiss and Infante Ferreira [39]. In this section, only the details required for the following steps of this paper will be discussed.

Fig. 1 depicts a schematic diagram of a single-effect absorption refrigeration/heat pump cycle. The system is mainly composed of an absorber (ABS), a generator (GEN), a condenser (CON), an evaporator (EVA), along with a solution heat exchanger (SHX), a pump and two throttle valves.

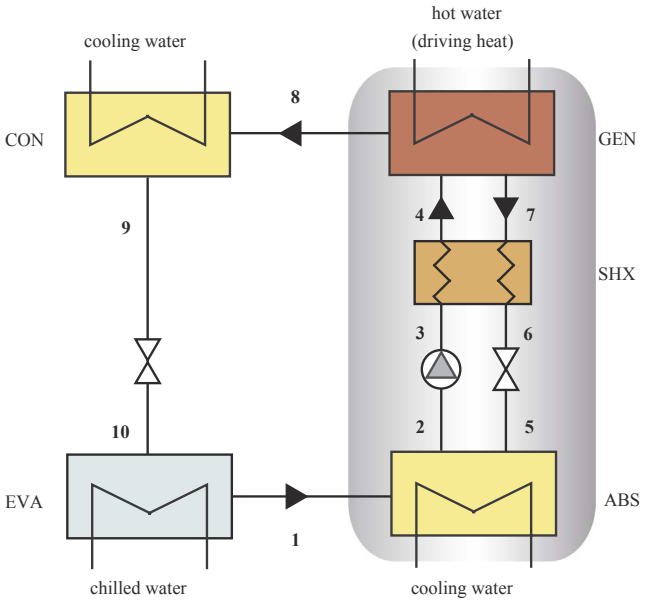

Fig. 1. Schematic diagram of a single-effect AHP system using IL based working pair.

To qualitatively illustrate the temperature and pressure relationship of each state, the process is also plotted in a $\ln P - (-1/T)$ diagram in Fig. 2. In the ABS, the weak NH_3/IL solution 5 (weak in the refrigerant, NH_3) absorbs the saturated pure NH_3 refrigerant vapor 1 from the EVA, and then it turns into strong solution 2. The heat Q_{abs} is delivered to the heating system by the ABS. The outlet solution 2 from the ABS is then pumped to a high pressure level and enters the SHX as a cold flow. The outlet flow of the cold side, stream 4, then goes into the GEN, where the driving heat Q_{gen} is input. With the heat input, strong solution 4 releases some refrigerant vapor 8, then becomes the poor solution 7 and enters the SHX. In the SHX, the weak solution 7 is cooled by the cold side to a state of 6 and then throttled to a low pressure level through a valve, before going back to the ABS. The superheated refrigerant vapor 8 from the GEN is condensed to a saturated pure liquid refrigerant in the CON, where the heat Q_{con} is delivered to the heating system. After that, the saturated liquid refrigerant 9 expands to a low pressure level through a valve, and extracts heat Q_{eva} from the surrounding in the EVA. The

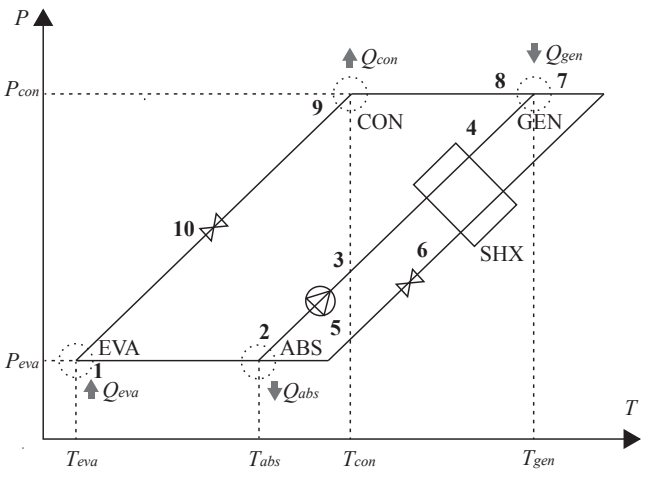

Fig. 2. The single-effect AHP cycle on a $\ln P - (-1/T)$ diagram.

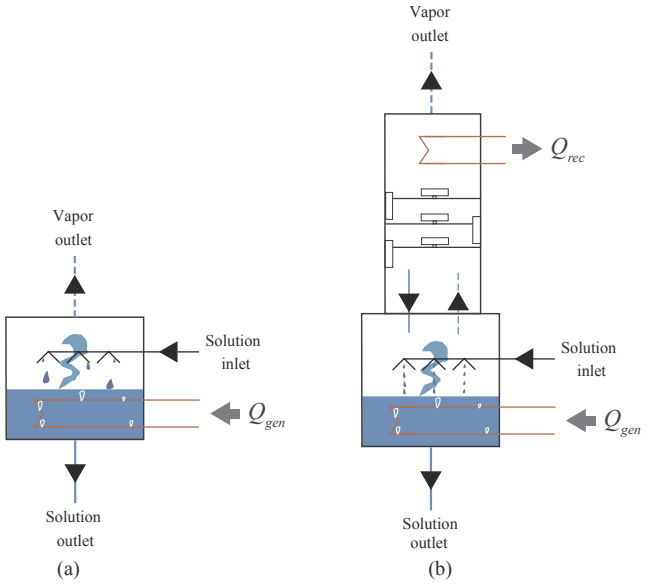

Fig. 3. Two constructions of the generator. (a) The generator for working pairs using absorbents with a negligible vapor pressure at operating temperature, say NH_3/ILs in this study. (b) The generator with purification section above it (distillation column and rectifier) for working pairs using absorbents with a non-negligible vapor pressure at operating temperature, say NH_3/H_2O in this study.

outlet vapor 1 goes back to the ABS and finishes the cycle.

In order to create an integrated model for the thermodynamic analysis of the absorption process with NH_3/ILs pairs, several assumptions are made to simplify the calculations:

- The system operates in a steady state.
- The heat losses, pressure losses and pumping work are neglected. The throttling is an isenthalpic process.
- The operating pressures of the EVA and the ABS are the same, and similarly, the pressures of the GEN and the CON are also equal.
- The minimum temperature approach of the solution heat exchanger, SHX, is set to 5 K.
- The refrigerant stream is saturated liquid or saturated vapor at the outlet of the CON or the EVA, respectively. The solution is at equilibrium state when leaving the GEN. While the solution leaving the ABS is subcooled, with a subcooling of 3 K.
- Vapor leaving the GEN is pure NH_3 which has the same temperature as the inlet solution (Fig. 3(a)).

The AHP system with an NH_3/H_2O pair is also modeled in this study for reference purposes. For it, an additional column and a rectifier are needed to purify the outlet vapor, as shown in Fig. 3(b). The reflux ratio must be iterated until an acceptable purity of the vapor outlet is obtained. Thus, additional simplification is taken into account,

- Vapor leaving the rectifier is pure enough (99.99% NH_3), and has a saturated temperature corresponding to the operating pressure (Fig. 3(b)). After the rectifier, it is treated as a pure fluid.

With the enthalpy of each state point, the heats exchanged in the EVA and the GEN are,

$$Q_{eva}/\dot{m}_r = h_1 - h_9 \tag{1}$$

$$Q_{gen}/\dot{m}_r = h_8 + f(h_7 - h_4) - h_7 \tag{2}$$

From the mass balance of the refrigerant in the solution,

$$\dot{m}_s(1-w_4) = (\dot{m}_s - \dot{m}_r)(1-w_7) \tag{3}$$

The performance parameters, i.e. circulation ratio (f) and COP can be calculated as,

$$f = \frac{\dot{m}_s}{\dot{m}_r} = \frac{1-w_7}{w_4-w_7} \tag{4}$$

$$COP = \frac{Q_{con} + Q_{abs}}{Q_{gen}} \tag{5}$$

2.2. Properties

2.2.1. Vapor-liquid equilibria for the NH_3/ILs binary solutions

Vapor-liquid equilibria describe the relationships between parameters *P-T-x*, which can be used to identified the state points in the cycle. NRTL models for the prediction of VLE of mixtures have been frequently reported in the literature, see for instance [39]. In this section, only the details required for the following steps of this paper will be discussed.

For the NH_3/IL system, due to the non-volatility of ILs, the equilibrium criterion is simplified as,

$$P = \gamma_{NH_3} x_{NH_3} P^{sat}_{NH_3} \tag{6}$$

here, $P^{sat}_{NH_3}$ can be obtained from NIST Refprop [40]. The activity coefficient γ_{NH_3} can be obtained through the NRTL activity coefficient model after correlating VLE data,

$$\ln\gamma_{NH_3} = x_2^2\left[\tau_{21}\left(\frac{G_{21}}{x_1 + x_2 G_{21}}\right)^2 + \frac{G_{12}\tau_{12}}{(x_2 + x_1 G_{12})^2}\right] \tag{7}$$

where,

$$\begin{cases} G_{12} = \exp(-\alpha\tau_{12}) \\ G_{21} = \exp(-\alpha\tau_{21}) \\ \tau_{12} = \tau_{12}^{(0)} + \frac{\tau_{12}^{(1)}}{T} \\ \tau_{21} = \tau_{21}^{(0)} + \frac{\tau_{21}^{(1)}}{T} \end{cases} \tag{8}$$

2.2.2. Enthalpies of the refrigerant and solutions

The enthalpy data of pure NH_3 are directly obtained from NISTs Refprop [40]. For a real solution, the total enthalpy can be estimated using the following method, depending on its state.

For a saturated solution at an equilibrium condition T, P and w_{NH_3}, the total enthalpy is,

$$h^{sol}(T,P,w_{NH_3}) = h^{sol}_{sat} = w_{NH_3}h_{NH_3}(T) + w_{IL}h_{IL}(T) + h^E(T,P,w_{NH_3}) \tag{9}$$

where the enthalpies of NH_3 are chosen at their saturated liquid states. For the ILs, the enthalpies are calculated with the help of their pure heat capacities C_p^{IL},

$$h_{IL}(T) = h_0(T_0) + \int_{T_0}^{T} C_p^{IL}\,dT \tag{10}$$

The calculation of the excess enthalpy, h^E, can be obtained using an

Table 1
Molecular weight and critical data of the investigated ILs.

ILs	*Mw* [kg kmol^{-1}]	T_c * [K]	P_c * [MPa]
[mmim][DMP]	222.18	816.8	2.72
[emim][BF_4]	197.97	596.2	2.36
[hmim][BF_4]	254.08	690.0	1.79
[omim][BF_4]	282.13	737.0	1.60
[bmim][BF_4]	226.02	643.2	2.04
[bmim][PF_6]	284.18	719.4	1.73
[emim][Tf_2N]	391.31	1249.3	3.27
[emim][$EtSO_4$]	236.29	1067.5	4.05
[emim][SCN]	169.25	1013.6	2.23

* The critical data are obtained using the group-contribution-function method [42].

equation of state (EOS) and mixing rules. Yokozeki and Shiflett [21,22,41] employed a modified Redlich-Kwong (RK) type of cubic EOS to fit the vapor pressure data and to predict the excess enthalpy. This method is also used for the prediction of the mixing heat in the present work. The detailed approach has been reported in the mentioned references. The values of the critical temperature and pressure of ILs needed for the following calculations, along with their molecular weights, are listed in Table 1.

For subcooled solutions at condition T, P and w_{NH_3}, its enthalpy can be obtained by subtracting the subcooled part from a corresponding saturated solution,

$$h^{sol}(T,P,w_{NH_3}) = h(T_{sat},P,w_{NH_3}) - \int_{T}^{T_{sat}} C_p^{sol} dT \quad (11)$$

In this study, the weighted average heat capacity of both components has been implemented to express C_p^{sol}.

$$C_p^{sol}(w_{NH_3}) = w_{NH_3} C_p^{NH_3} + (1-w_{NH_3}) C_p^{IL} \quad (12)$$

This treatment has been verified for H_2O/[mmim][DMP] with C_p^{sol} data in [15] showing that the relative deviation is always smaller than 4%.

If T of a stream is higher than T_{sat}, part of the NH_3 in the solution will be boiled off. For this case, the total enthalpy can be expressed as,

$$h^{sol}(T,P,w_{NH_3}) = (1-q) h_{sat}^{sol} + q h^{vap} \quad (13)$$

where, h_{sat}^{sol} and h^{vap} are the specific enthalpies for the saturated solution part and the vapor part, respectively. q is the quantity, which can be identified as,

$$q = \frac{w - w_{sat}}{1 - w_{sat}} \quad (14)$$

2.3. Optimization problem

The properties of ILs can be adjusted by the design of anion and cation combinations for a task-specified purpose. However, because of the large number of anions and cations, the number of possible combinations is considerable. In this paper, the determination of screen criteria of task-specific ILs for AHPs will also be discussed. These criteria are identified via the optimization of the cycle performance.

In the optimization, the objective is the maximization of the COP which depends on solubility (concentration of weak and strong solutions) and enthalpy values as will be discussed in Section 3.5. Making use of an NRTL model, a total of eight parameters are identified which affects the attained COP value. They are α, $\tau_{12}^{(0)}$, $\tau_{12}^{(1)}$, $\tau_{21}^{(0)}$ and $\tau_{21}^{(1)}$ of the NRTL model for VLE, c_0, c_1 in linear molar C_p expression and the molecular weight *Mw*. Once the COP reaches the optimal value, corresponding optimal variables can be determined for the optimum IL and mixture. Meanwhile, in order to obtain a practical and reasonable result, constraints of these optimal variables are needed. They are determined in terms of experimental data which are collected and discussed in Section 3.1.

The GA is better at finding global solutions than gradient-based solvers. GA selectively generates new candidate points to evaluate based upon a method that is similar to breeding between two "parents" to generate a "child". They are useful for problems that are highly nonlinear, such as the present problem. One of the concerns is the computational efficiency. To check a large amount of individuals from generation to generation is time-consuming. Luckily, the present optimization problem is not so CPU-intensive. In addition, the selection of individuals in the current generation is random, which can also lead to local minima. To overcome this drawback, instead of using GA for only one optimization, we try thousands of optimizations based on GA independently to remove local minima. The non-physical optimization results will be rejected. Finally, the optimum value for the objective function can be identified. The GA toolbox of Matlab has been used to identify the optimum combination of parameters. The effect of the settings for what concerns population size, elicit count, crossover fraction and generations has been investigated by studying the effect of variations and finally the settings proposed in the Matlab toolbox, respectively, 200, 10, 0.8 and 500, have been adopted.

3. Results and discussion

3.1. Correlations and summaries of properties

3.1.1. Vapor liquid equilibria

With the experimental VLE data of binary NH_3/ILs, the binary parameters, α, $\tau_{12}^{(0)}$, $\tau_{12}^{(1)}$, $\tau_{21}^{(0)}$ and $\tau_{21}^{(1)}$ of the NRTL model (Eq. (7) and (8)), can be correlated and will allow for the determination of the operating concentrations. The correlated results and accuracies are listed in Table 2. In this work, most of the data have been correlated with a root-mean-square deviation (RMSD) smaller than 5.62% as shown in Table 2. Only the model for the pair NH_3/[omim][BF_4] showed slightly larger deviation: 8.7%.

3.1.2. Heat capacities

Experimental heat capacity (C_p) data of 61 ILs at 298.15 K, reviewed by Paulechka [46], are plotted in Fig. 4 in mole-based and mass-based units, respectively. It is quite interesting to see that the mole-based C_p data are distributed in a linear trend with respect to the molecular weight. The mass-based C_p data are centralized near 1.44 kJ kg^{-1} K^{-1} in a nearly constant range between 1 and 2 kJ kg^{-1} K^{-1}. This trend provides a general relationship between C_p and *Mw* for ILs, which will be used in the property optimization as a constraint. Even though the relationship is not very accurate, it still can be helpful to identify how this property impacts on the performance of the mixture in the AHP.

For the same ILs involved in the NRTL correlation in Table 2, the mole-based C_p values are also plotted as a function of temperature in

Table 2
Correlated binary parameters in the NRTL model for the investigated working pairs.

Working pairs*	α	$\tau_{12}^{(0)}$	$\tau_{12}^{(1)}$	$\tau_{21}^{(0)}$	$\tau_{21}^{(1)}$	Data points	RMSD**
NH_3/[mmim][DMP][1]	0.24032	7.82	−2300.68	−4.43	1000.39	30	3.31%
NH_3/[emim][BF_4][2]	0.99952	−0.01	236.41	−1.26	164.59	25	5.14%
NH_3/[hmim][BF_4][3]	0.99998	−14.8	5081.74	−2.67	478.85	25	4.29%
NH_3/[omim][BF_4][4]	0.90702	−7.01	2690.74	−2.4	283.17	25	8.71%
NH_3/[bmim][BF_4][5]	−0.01285	−48.23	8961.06	32.62	−5490.64	30	2.62%
NH_3/[bmim][PF_6][6]	0.33411	3.73	−509.57	−4.19	643.5	29	2.98%
NH_3/[emim][Tf_2N][7]	−0.00422	−100	14710.17	71.51	−9046.21	30	5.62%
NH_3/[emim][$EtSO_4$][8]	0.71604	11.17	−4089.25	−7.53	2451.46	29	4.32%
NH_3/[emim][SCN][9]	−0.27082	−10.66	3120.01	5.6	−1967.71	36	4.59%
NH_3/H_2O[10]	−0.24355	24.17	-18636.43	7.26	-3370.40	111	3.24%

* The experimental VLE data used are from, [1] [43], [2], [3] and [4] [44], [5], [6] and [7] [21], [8] and [9] [22] and [10] [45]. Data of the NH_3/H_2O pair are used as a reference.
** RMSD is obtained based on the deviations between the correlated and experimental pressure data by $RMSD(P) = \sqrt{\frac{\sum_N (P_{flt}/P_{exp} - 1)^2}{N}}$.

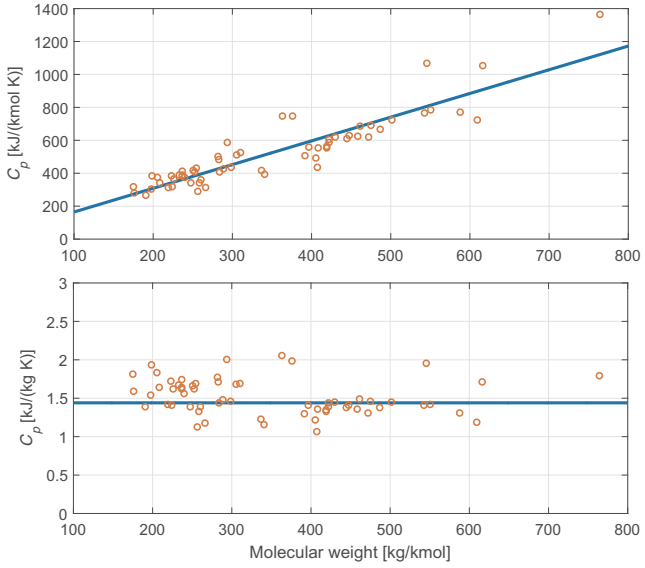

Fig. 4. C_p values of 61 ILs at 298.15 K (upper: mole-based, lower: mass-based). These 61 data points have been collected from experimental C_p data reviewed by Paulechka [46]. They are selected because they are the only ones having C_p data at 298.15 K with uncertainties lower than 15%.

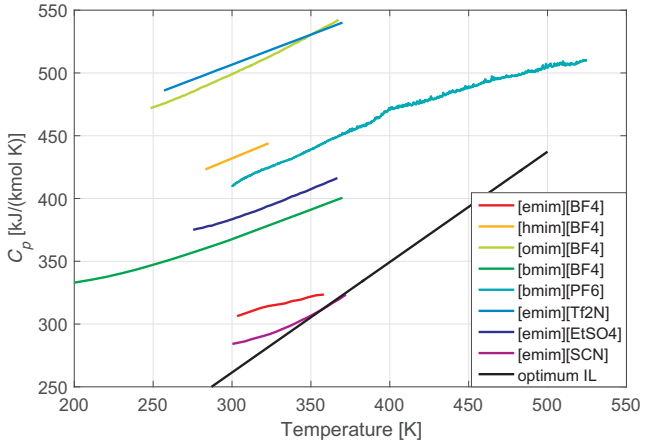

Fig. 5. Experimental C_p (mole-based) values of the investigated ILs as a function of temperature.

Table 3
Correlated parameters in C_p [kJ kmol^{-1} K^{-1}] = $c_0 + c_1 T$[K] (mole-based) for the investigated ILs.

ILs*	c_0	c_1	Data points	RMSD
[mmim][DMP][1]	−153.898	1.476	4	0.94%
[emim][BF_4][2]	214.067	0.308	12	0.18%
[hmim][BF_4][3]	275.962	0.520	9	0.00%
[omim][BF_4][4]	323.894	0.588	100	0.21%
[bmim][BF_4][5]	250.201	0.397	20	0.68%
[bmim][PF_6][6]	282.070	0.452	1528	0.91%
[emim][Tf_2N][7]	363.188	0.478	16	0.01%
[emim][$EtSO_4$][8]	245.526	0.462	146	0.60%
[emim][SCN][9]	116.474	0.547	20	0.61%

* The experimental C_p data used are from, [1] [47], [2] [48], [3] [49], [4], [5] and [8] [50], [6] [51], [7] [52] and [9] [53].

Fig. 5. With respect to the temperature, the C_p values of different ILs also show approximately linear trends. Thus, the molar C_p value of each IL is represented by a linear expression. Table 3 lists the correlated parameters of the linear expression and is based on the experimental C_p data from literature [47–53]. The accuracies of all correlations are also listed. Notice that for most fluids the available data are limited to 100 °C, so that the relation is extrapolated when calculating values up to 130 °C. This may lead to larger errors than reported in Table 3.

3.2. Performance comparison

To compare the performances in detail, some calculated results are listed in Table 4 at a specific condition ($T_{gen}/T_{con}/T_{abs}/T_{eva}$ = 120/45/45/10 °C). This operating conditions range is specified based on applications in floor heating. Apart from the solubility levels of the in- and outlet of the ABS and performance parameters f and COP, the conditions at the GEN inlet (state point 4) are also checked. Qualities q_4 are listed to show if there is vapor boiled-off before entering the GEN. The table also includes the results for the NH_3/H_2O system and optimum results obtained in Section 3.5. The single-effect AHP cycle with NH_3/H_2O as working fluids, reported by Kotenko [23], operates at similar conditions as applied in the current work. His predicted heating COP for a system with a rectifier and slightly lower evaporating temperature (T_e = 5 °C) is around 1.59, which is quite close to the values obtained in the current work of 1.61.

Two facts resulting from the circulation ratio, f, can influence the cycle performance. One is its impact on the pumping power. A higher value of f means a larger mass flow rate through the pump (at the same flow of refrigerant stream), which can increase the power consumption of the solution pump. The second one is due to the relationship between f and the energy and mass balances for the GEN and for the ABS, which will be discussed in detail in Section 3.3. In all, a small f is preferable. Because of the significant difference in molecular weights between NH_3 and ILs, the mass concentrations of NH_3/ILs pairs are much lower than that of the NH_3/H_2O system. As a result, the circulation ratios of NH_3/ILs mixtures (29.2–112.3) are significantly higher than that of conventional NH_3/H_2O (4.6). Promisingly, 4 of the ILs based systems hold higher COP values than that for the NH_3/H_2O system (1.61). These ILs are [mmim][DMP] (1.79), [emim][Tf_2N] (1.74), [emim][SCN] (1.73) and [bmim][BF_4] (1.70). Although the performance of the NH_3/H_2O system could be improved by implementing advanced cycles, such as the generator/absorber heat exchanger (GAX) cycle, that would also increase the complexity and investment of the system. These promising results show the potential of NH_3/ILs working pairs which can be executed with a simple cycle, making these pairs superior alternatives.

Previously Yokozeki and Shiflett [21,22] have compared the performance of some of the investigated mixtures in single-effect absorption refrigeration cycles. Their results are also included in Table 4 for reference. At their considered operations conditions, the NH_3/H_2O pair has been identified to perform better than the considered NH_3/ILs pairs. This is different from the current work, in which the NH_3/H_2O pair is not identified as the superior one for a heat pump operation. Yokozeki and Shiflett [21,22] did not include the effect of the rectifier when calculating the performance of the NH_3/H_2O pair. The rectifier is essential to guarantee the purity of the produced refrigerant. This is the main reason why their COP of the NH_3/H_2O pair was overestimated. Besides, although the experimental VLE data of Yokozeki and Shiflett [21,22] have been used for these fluids in the present work, the NRTL parameters have been independently correlated. The fitted VLE behaviors are not identical but quite similar to the ones reported by Yokozeki and Shiflett [21,22]. The difference in COP results for the NH_3/IL pairs is mainly due to the method used to predict the specific heat of the working pairs. For example, Yokozeki and Shiflett [21,22] made use of the group contribution function method to predict these values, while in this study the reported experimental values have been used as discussed in Section 3.1. Problems encountered when using the group contribution function method for the prediction of the specific heat of ionic liquids have previously been reported by Cai et al. [20], as already

Table 4
Performance comparison when different working pairs are used in the AHP cycle ($T_{gen}/T_{con}/T_{abs}/T_{eva}$ = 120/45/45/10 °C) and the refrigeration COP ($T_{gen}/T_{con}/T_{abs}/T_{eva}$ = 100/40/30/10 °C) of corresponding pairs from Yokozeki and Shiflett [21,22].

Working pairs	Heat pump performance*					Refrigeration performance	
	w_2 [kg kg^{-1}]	w_7 [kg kg^{-1}]	q_4 [kg kg^{-1}]	f [–]	COP [–]	f [–]	COP [–]
NH_3/[mmim][DMP]	0.057	0.031	0.017	36.614	1.785	–	–
NH_3/[emim][BF_4]	0.054	0.034	0.011	46.824	1.609	–	–
NH_3/[omim][BF_4]	0.080	0.072	0.002	112.370	1.381	–	–
NH_3/[bmim][BF_4]	0.057	0.023	0.014	29.282	1.695	12.98	0.557
NH_3/[bmim][PF_6]	0.061	0.046	0.006	63.077	1.461	17.27	0.575
NH_3/[emim][Tf_2N]	0.043	0.025	0.007	54.303	1.736	24.57	0.525
NH_3/[emim][$EtSO_4$]	0.056	0.039	0.010	55.542	1.509	17.55	0.485
NH_3/[emim][SCN]	0.082	0.049	0.015	29.238	1.732	12.42	0.557
NH_3/H_2O	0.481	0.335	0.024	4.555	1.612	2.54	0.646
NH_3/optimum IL	0.908	0.013	–	1.102	1.836	–	–

* Concentration data are all for the NH_3 component. The subscript 2 and 7 represent outlet conditions of the ABS and the GEN, respectively, which are locations with strong and weak solution flows. The subscript 4 represents the inlet conditions of the GEN.

discussed in the introduction.

3.3. Contributions to the generation heat

Considering the energy balance of the 4 main devices, the COP of a heat pump system can also be expressed as,

$$COP = \frac{Q_{abs} + Q_{con}}{Q_{gen}} = \frac{Q_{eva} + Q_{gen}}{Q_{gen}} = 1 + \frac{Q_{eva}}{Q_{gen}} \tag{15}$$

The EVA heat, Q_{eva}, is equal for all fluids. Thus, the difference in COP results from the GEN heat, Q_{gen}: A higher Q_{gen} leads to a lower heat pump COP.

To make this clear, relevant expressions of the total enthalpies in Section 2.2 along with Eq. (4) and (14) are substituted into Eq. (2). Taking into account the heat and mass balances of the GEN, the heat input in the GEN, Q_{gen}, can be rewritten as,

$$\begin{aligned} Q_{gen}/\dot{m}_r &= (1-fq)[h_8-(h_{NH_3})_{4,sat}] \\ &+ [(f-1)(h^E)_7-f(1-q)(h^E)_{4,sat}] \\ &+ (f-1)(w_{NH_3})_7[(h_{NH_3})_7-(h_{NH_3})_{4,sat}] \\ &+ (f-1)(w_{IL})_7[(h_{IL})_7-(h_{IL})_{4,sat}] \end{aligned} \tag{16}$$

Q_{gen} is split into 4 terms in this expression. The first term is the latent heat effect from the condensation of NH_3 vapor (while also includes the sensible heat associated with the superheated state, while very small). The second one denotes the excess heat. The other two terms represent the contributions of sensible heat, in which, the term in the third line is the sensible heat change of the NH_3 component while the term in the last line is that of the IL component.

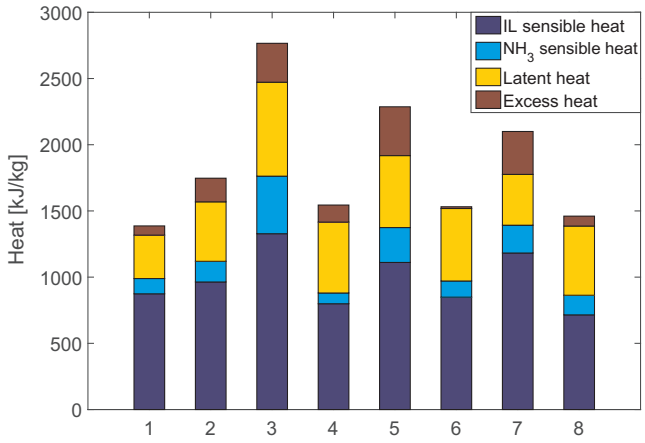

Fig. 6. Contributions to the GEN heat Q_{gen} by the 4 terms of Eq. (16). The 4 terms are latent heat, absorption heat and sensible heats of both components. 1–8 denotes NH_3 based working fluids with [mmim][DMP], [emim][BF_4], [omim][BF_4], [bmim][BF_4], [bmim][PF_6], [emim][Tf_2N], [emim][$EtSO_4$] and [emim][SCN].

In order to analyze the performance, each of the above contributions to the GEN heat, for the operating condition $T_{gen}/T_{con}/T_{abs}/T_{eva}$ = 120/45/45/10 °C, is depicted in Fig. 6 for all the NH_3/ILs working pairs.

The values of T_4 are almost identical for all the cases, indicating that the latent heats per unit mass flow, $h_8-(h_{NH_3})_{4,sat}$, are more or less the same for all cases. The difference in latent heat in Fig. 6 is due to the different mass flows, $1-fq$. Large values of f or q can lead to a low value of the latent heat contribution. The q has an obvious negative correlation with the latent heat contribution, which can be observed in Fig. 6, e.g. pairs with [omim][BF_4] and [bmim][PF_6]. A higher q implies more vapor is boiled off before the flow enters the GEN. In this way, the heat duty of the GEN is reduced. The q value results mainly from the VLE properties of the NH_3/ILs systems.

Again, due to the almost equal values of T_4, the sensible heats per unit mass flow from NH_3 component are identical for all the mixtures. The difference in NH_3 sensible heats is mainly caused by the factor, $(f-1)(w_{NH_3})_7$. Also the circulation ratio, f, has a stronger impact compared with $(w_{NH_3})_7$. This is also true for the contribution of the sensible heat of the ILs: since the mass-based C_p values of ILs and temperature differences between inlet and outlet ΔT are approximately the same, the sensible heat of the ILs per unit mass flow, $C_p\Delta T$, are similar for all the ILs. The difference in sensible heat contributions is mainly due to the required circulation ratio, f. Smaller f of pairs with [bmim][BF_4], [emim][Tf_2N] and [emim][SCN] lead to smaller sensible heat contributions and correspondingly higher COPs. This indicates that the circulation ratio f is dominant in this case. The solubility difference at the in- and outlet of the ABS will determine the f values.

Since the VLE properties are usually studied with mole-based units, when considering mass-based properties, say f here, Mw also plays a role. For the NH_3 absorption system, a larger molecular weight of the absorbent leads to a smaller mass concentration change when the molar change is maintained. This also implies that smaller molecular weight of the absorbent is preferable in terms of performance.

The contribution of excess heat will be discussed in Section 3.4.

3.4. Influence of heat source temperature on the performance

To investigate the influence of heat source temperature on the performance, condensing temperature T_{con}, absorbing temperature T_{abs} and evaporating temperature T_{eva} are set to be 45 °C, 45 °C and 10 °C, respectively, while the temperature of the heat source, T_{gen}, varies in a range from 100 °C to 130 °C. Because all the experimental VLE conditions are lower than 130 °C, T_{gen} is maintained below 130 °C in all calculations.

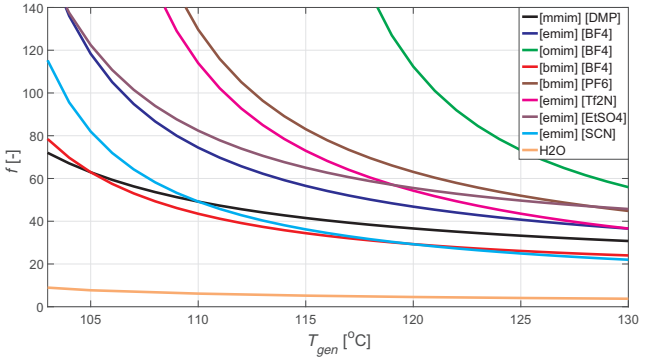

Fig. 7. Circulation ratios, *f*s, with respect to generation temperature for the NH_3/IL based working pairs in the single-effect AHP cycles at the condition of $T_{con}/T_{abs}/T_{eva}$ = 45/45/10 °C.

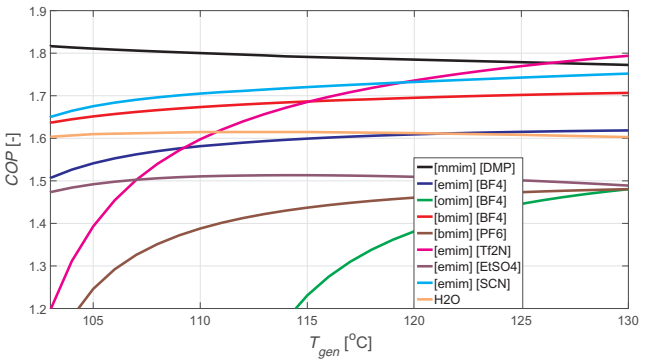

Fig. 8. COPs with respect to generation temperature for different NH_3/IL based working pairs in the single-effect AHP cycles at the condition of $T_{con}/T_{abs}/T_{eva}$ = 45/45/10 °C.

Under these operating conditions, the circulation ratio *f* of the NH_3/[hmim][BF_4] working pair always has a negative value, what means this pair cannot operate in an AHP which operates under the imposed conditions. Thus, Figs. 7 and 8 only show the circulation ratio *f* and COP variation, respectively, for the other 8 NH_3/ILs pairs and NH_3/H_2O pair. All the working pairs, considered for the proposed AHP system, show similar trends. With increase of T_{gen}, *f* first decreases rapidly and then reduces to a more constant value. On the contrary, the COPs increase first sharply and then rise to a relatively constant value. At the higher temperature range, the values of *f* and COP are quite close for most NH_3/ILs pairs. *f* falls in the range of 20–60 and COPs reach 1.4–1.8. It looks like these trends will be maintained when T_{gen} increases above 130 °C.

The performances of working pairs with [mmim][DMP], [bmim][BF_4], [emim][Tf_2N] and [emim][SCN] are quite outstanding just as shown in Section 3.2 at a constant condition. Even though the *f*s of these points are larger than that of NH_3/H_2O, when T_{gen} is high enough, the COPs are still higher. In addition, the NH_3/[mmim][DMP] pair has the highest COP.

As for the NH_3/H_2O pair, it holds the lowest *f* and relatively high COP values when compared with the NH_3/ILs pairs. With an increase of T_{gen}, the COP slightly rises, and after 105 °C, it becomes more or less constant.

Because an accurate prediction of the excess enthalpy is difficult as discussed in Section 1, and to assess the sensitivity of excess enthalpy on the performance, COPs calculated based on ideal solutions (without taking account the excess enthalpy) are presented in Fig. 9.

In these cases, the range of the COP is smaller than when the excess enthalpy is taken into account. Even though the COP values are now lower, the working pairs, which show a better performance than that of NH_3/H_2O pair in Fig. 8, still perform better when the excess enthalpy

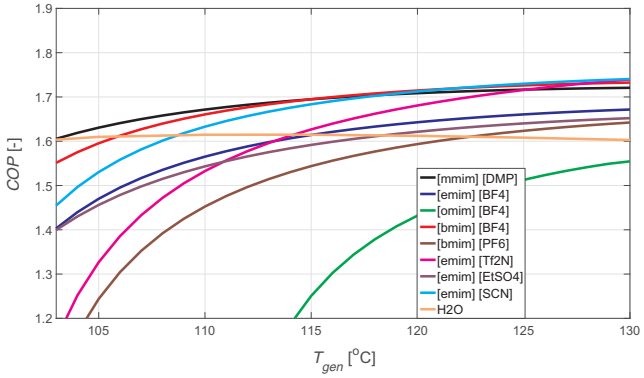

Fig. 9. COPs with respect to generation temperature for different NH_3/IL based working pairs in the single-effect AHP cycles when the excess enthalpy is not taken into account, at the condition of $T_{con}/T_{abs}/T_{eva}$ = 45/45/10 °C.

contribution is neglected. An accurate measurement is still needed for a better assessment of the excess enthalpy of NH_3/IL pairs in AHPs.

3.5. Optimum performance and corresponding properties

In the optimization work, the molecular weight is assumed in a range 170–400 kg/kmol. Taking the previous correlation results into account, the upper and lower limits of the thermodynamic model parameters are summarized in Table 5. Based on these, and the linear relationships of C_p with both molecular weight and temperature as discussed in Section 3.1, the constraints of the search domain have been defined.

The property optimization work is conducted under the same operating conditions as discussed in Section 3.2, i.e. $T_{gen}/T_{con}/T_{abs}/T_{eva}$ = 120/45/45/10 °C, for the application of building's floor heating.

Using the GA method, the optimized performance and corresponding optimum variables are obtained and listed in Table 6. The maximum COP under above constraints could reach 1.836 and the circulation ratio 1.102.

The *P-T-x* diagram of the optimum IL/NH_3 mixture described by the parameters of the NRTL model is shown in Fig. 10. As a comparison, the *P-T-x* diagram of NH_3/[emim][SCN] is also plotted. Generally, the vapor pressure of the optimum pair has a large deviation between the low and high temperature range. For the optimum working pair, there is a negative deviation effect from the Raoult's law at the low temperature range while a positive deviation applies at the high temperature range. This absorption capability difference causes a large difference of NH_3 concentration between in and outlet of the ABS, what will lead to a smaller *f*, and a higher COP.

The optimum molecular weight *Mw* is exactly its lowest limit, 170. For the same molar solubility difference, a lower value of *Mw* will lead to a higher value of mass solubility difference which will then lead to a lower *f* and a higher COP. Besides, since the molecular weight *Mw* has a linear ascending relationship with mole-based C_p, correspondingly, a lower mole-based C_p is observed for the optimum IL, which is depicted in the lowest position in Fig. 5.

The optimum properties including vapor pressure, C_p and *Mw* allow us to screen the ideal ILs for AHP cycles. The challenge for future work is identifying ILs which show properties close to the *Mw*,C_p and vapor pressure of the optimized ideal mixture. It is clear that a low molecular weight, low C_p and large concentration difference between in- and outlet of the ABS are essential requirements.

3.6. Outlook of economic and technical feasibilities

In an economic analysis, the COP values are related to the operational costs of the AHP while the capital costs are related to the

Table 5
Limits of optimization variables and properties in the optimization problem.

Variable	α	$\tau_{12}^{(0)}$	$\tau_{12}^{(1)}$	$\tau_{21}^{(0)}$	$\tau_{21}^{(1)}$	c_0	c_1	C_p [kJ kg^{-1} K^{-1}] at 298.15 K	M_w[kg kmol^{-1}]
Lower limit	−1	−200	−5000	−10	−10000	−1000	0	1.3	170
Upper limit	2	100	15000	100	2500	100	1000	2	400

Table 6
Optimized performance & optimum variables of the working fluids in the single-effect AHP at a condition of $T_{gen}/T_{con}/T_{abs}/T_{eva}$ = 120/45/45/10 °C.

Performance		NRTL					C_p [kJ kmol^{-1} K^{-1}]		*Mw*
COP	f	α	$\tau_{12}^{(0)}$	$\tau_{12}^{(1)}$	$\tau_{21}^{(0)}$	$\tau_{21}^{(1)}$	c_0	c_1	[kg kmol^{-1}]
1.836	1.102	1.171	8.898	14147.7	23.557	-8759.68	−39.966	0.875	170

investment in equipment and working fluids. To determine the sizes of the main components, which are the heat exchangers, the duty and overall heat transfer coefficient of each main heat exchanger are first estimated taking the local flow and fluid properties into account. A conventional NH_3/H_2O AHP with shell-and-tube HXs is here compared with an NH_3/IL AHP. IL [emim][SCN] is selected as absorbent for the NH_3/IL AHP since it is one of the best performing ILs and because its viscosity and current price are the lowest among the studied ILs as shown in Table 7.

Boman et al. [37] have recently shown that the IL-based AHP systems need more heat exchanger area due to the poor heat transfer performance of the ILs, caused by their higher viscosity, lower thermal conductivity and heat capacity. In this section, PHXs are considered in the IL based absorption systems in the roles of GEN, ABS, SHX, CON and EVA. The PHX is selected mainly due to its compact size and good performance of heat and mass transfer. The compact design of PHXs keeps the system volume small so that a smaller amount of expensive working fluid is sufficient to fill the system.

3.6.1. Equipment sizing

The floor heating system for a building in a moderate climate area, for example, the Netherlands, is taken for the economic comparison of the AHPs. The heating load will generally not exceed 60 W/m^2 [59]. A 3750 m^2 building will have a heating capacity of 225 kW and its yearly heating requirement will be, approximately, 337.5 MW h.

PHX with plate sizes 0.191 × 0.618 m (width × length) and plate spacing of 1.5 mm have been considered for all heat exchangers except for the SHX. The dimensions of the SHX were 0.390 × 0.990 m with an identical plate spacing.

The overall heat transfer coefficient for each heat exchanger has been

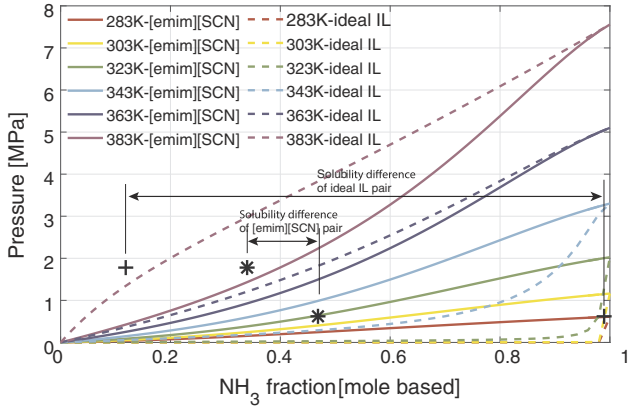

Fig. 10. Comparison of the *P-T-x* behavior between the optimized NH_3/IL pair and the real pair (NH_3/[emim][SCN]).

Table 7
Viscosities and prices of the most promising commercialized ILs for single-effect AHPs in this study.

ILs*	Viscosity at 25 °C [Pas]	Viscosity at 90 °C [Pas]	Price [€ kg^{-1}]
[mmim][DMP][1]	0.291	–	910
[bmim][BF_4][2]	0.106	0.0099	846
[emim][Tf_2N][3]	0.0339	0.0056	1265
[emim][SCN][4]	0.0245	0.0055	703/172**
58.5 wt% LiBr aqueous solution[5]	0.0068	0.0022	-

* Price data are collected from vendors of ILs. The data of viscosities are from: [1] [54], [2] [55], [3] [56], [4] [57] and [5] [58].
** Different prices are offered by two different vendors.

obtained by summing the heat transfer resistances on both sides of the heat exchangers. The local heat transfer coefficient for single phase flows (both of external fluid and working fluid) has been predicted making use of the correlation proposed by Yan et al. [60]. Similarly, for the evaporation processes the correlation proposed by Khan et al. [61] and for the condensation processes the correlation proposed by Thonon and Bontemps [62] have been used. For the GEN and ABS the smallest value obtained considering single phase flow or, respectively, evaporation and condensation have been adopted so that mass transfer resistance is taken into account. The required heat exchanger area follows from the heat exchanger duty, its overall heat transfer coefficient and the logarithmic mean temperature difference between the two fluids.

The properties of the external fluid (water) and of NH_3 have been obtained from Lemmon et al. [40]. The properties of [emim][SCN] have been obtained from Freire et al. [57] (density and dynamic viscosity), Navarro et al. [53] (heat capacity) and Tenney et al. [63] (thermal conductivity). Table 8 shows the calculated areas for the different heat exchangers. For the SHX of the NH_3/IL system two options have been considered: a minimum temperature approach of 5 K (option 1) and a minimum temperature approach of 16 K (option 2). In this case the COP drops from 1.73 (option 1) to 1.54 (option 2) while the required PHX area significantly reduces.

3.6.2. Economic analysis

For the economic calculation, a cost equation based on DACE [64] PHX costs has been applied to the areas reported in Table 8:

$$C_{phx} = 1.934A^{0.6233} \tag{17}$$

with C_{phx} expressed in k€ and A expressed in m^2, for the SS316 PHX in the area range of 40 to 300 m^2. The cost of SS316 shell-and-tube HXs is taken from the same source for the area range of 30 to 200 m^2.

$$C_{sthx} = 3.743A^{0.5948} \tag{18}$$

Table 8
Equipment size for both AHP systems, based on the same conditions applied in Table 4.

Component	NH_3/[emim][SCN]				NH_3/H_2O		
	Heat duty [kW]	OHTC* [W m^{-2} K^{-1}]	Area [m^2]	Plates number [–]	Heat duty [kW]	OHTC [W m^{-2} K^{-1}]	Area [m^2]
GEN	129.9	2390	2.7	39	138.4	1700	4.1
ABS	111.7	3010	2.3	33	138.3	880	6.8
REC	–	–	–	–	21.2	800	2.2
EVA	95.1	6980	2.1	31	85.5	820	16.2
CON	113.3	5870	1.4	21	86.7	700	8.9
SHX (option 1)**	354.8	300	134.7	856	87.6	610	11.7
SHX (option 2)	292.6	400	53.9	233	–	–	–

* The OHTC stands for the Overall heat transfer coefficient.
** Option 1 denotes a SHX with a minimum temperature approach of 5 K. Option 2 denotes a SHX with a minimum temperature approach of 16 K.

Table 9
Yearly energy requirements and yearly capital costs of the different AHP systems in comparison to a conventional boiler.

	Heating efficiency [–]	Primary energy demand [MW h]	Primary energy cost [k€]	Yearly HX cost [k€]	Yearly work fluid cost* [k€]	Total yearly cost [k€]	Yearly savings** [%]
Boiler	0.85	397	21.8	–	–	21.8	–
AHP NH_3/IL (option 1)	1.47	229	12.7	2.8	29.3 7.2 0.1	44.7 22.6 15.5	−105.0 −3.6 28.9
AHP NH_3/IL (option 2)	1.31	258	14.3	1.6	8.1 2.0 0	23.8 17.7 15.7	−9.2 18.8 28.0
AHP NH_3/H_2O	1.37	246	13.7	2.5	–	16.0	26.6

* Three different costs in the case of NH_3/[emim][SCN] pairs corresponding to three different prices adopted in the analysis.
** The negative of the yearly saving indicates extra costs.

The yearly HX costs take into account a (linear) depreciation time of 15 years. The price of natural gas for households and commercial consumers has been taken as 55 €/MW h [65]. A boiler efficiency of 85% has been adopted, which has also been taken into account for the other AHP systems. The price of IL varies significantly depending both on production amounts and manufacturing technique. The prices of the [emim][SCN] listed in Table 7 are based on quotations in a lab scale production. It is also reported that, in large scale production, some ILs cost will reduce to 3.00 $/kg [66]. Honeywell UOP [67] reports the use of ILs to produce high-octane motor fuels and claims it is a “cost-effective solution”. This indicates that the application of ILs at an industrial scale does make their price economically more competitive. The values from the current vendors and the expected low value (3.00 $/kg) have been adopted in the present calculations. Table 9 shows the results of the economic comparison between the different AHP solutions and the use of a conventional boiler. All considered AHP options lead to both energy savings and costs savings, when the cost of IL is at a reasonable level (industrial scale production). The influence of the IL price is also shown. The NH_3/IL AHP with a large minimum temperature approach in the SHX performs economically the best for current IL prices.

3.6.3. Other technical concerns

STABILITY Most ILs have been reported as being stable as liquids over a very wide temperature range. It has also been reported for some NH_3/IL mixtures that chemical reactions take place [24]. Chemical reactions make the cycles less reversible. The long term operation of these fluids might be a concern but NH_3/IL mixtures which do not undergo chemical reactions are expected to be capable of realizing a large number of operational cycles in a reliable way.

VOLATILITY There have also been concerns about the negligible vapor pressure of ionic liquids [68]. Although being small, very small concentrations of IL vapor may leave the generator and enter the condenser. After a large number of cycles, IL may accumulate in the evaporator requiring additional actions to bring it back to the absorbent loop. Since no long term operation with these cycles has been reported, the practical performance of these mixtures still needs to be confirmed.

4. Conclusion

After a review of methods and a summary of available experimental properties, a thermodynamic model has been proposed to investigate single-effect AHPs with NH_3/ILs working pairs as working fluids for the purpose of the floor heating of buildings. With this model, the performance of the AHPs has been calculated for all 8 feasible NH_3/ILs pairs (one additional pair cannot operate under the considered conditions) and also for NH_3/H_2O. Additionally, a properties optimization work and economic analysis have been executed. Based on the work, the following conclusions could be drawn:

- The circulation ratio *f* decreases and COP increases with an increase of the generator temperature (up to 130 °C).
- Under the considered conditions, the COP of the NH_3/[mmim][DMP] pair reaches the best performance (COP of 1.79), and along with NH_3/[bmim][BF_4], NH_3/[emim][Tf_2N], NH_3/[emim][SCN] all showing a higher COP than that of the NH_3/H_2O pair. Nevertheless, the circulation ratio *f* is significantly higher than that for the NH_3/H_2O pair.
- The analysis of the generator heat requirement revealed that, high vapor quality values at the inlet of the GEN resulted in a high COP because of a lower latent heat contribution. The influence of circulation ratio, *f*, is mainly associated with the two sensible contributions (the sensible heat of both components), and a low *f* would lead to a high COP. Neglecting the excess enthalpy, the performance changes, but the better working pairs still beat NH_3/H_2O pair in terms of COP.
- The optimum COP of this type of working pairs and for the condition

considered can be expected to reach 1.84 as demonstrated by the property-optimization study.

- To realize an ideal performance, the optimum IL candidates should show high absorption capabilities, large solubility differences between in- and outlet of the generator, low molecular weights and low heat capacities. The optimization study shows its potential to assist in the selection of IL as absorbents.
- Large circulation ratio combined with worse heat transfer performance in the solution heat exchanger lead to large demand of heat transfer area, which additionally requires a large amount of expensive ILs.
- An economic feasibility analysis indicates that, when the [emim][SCN] would be produced at industrial scales, this NH_3/IL AHPs lead to both significant energy (42%) and economic (29%) savings.

Acknowledgment

The authors would like to acknowledge the financial support from the China Scholarship Council.

References

[1] International Energy Agency. Energy, Climate Change & Environment - 2016 Insights. Tech. rep., OECD/IEA, Paris; 2016.
[2] EU Commission. Communication from the Commission to the European Parliament, the Council, the European Economic and Social Committee and The Committee of the Regions, An EU Strategy on Heating and Cooling. Tech. rep., Brussels; 2016.
[3] U.S. Department of Energy. 2011 Buildings Energy Databook. Tech. rep.; 2012.
[4] Tsinghua University Building Energy Research Center, International Energy Agency. Building Energy Use in China Transforming Construction and Influencing Consumption to 2050. Tech. rep., OECD/IEA, Paris; 2015.
[5] Medrano M, Bourouis M, Coronas A. Double-lift absorption refrigeration cycles driven by low-temperature heat sources using organic fluid mixtures as working pairs. Appl Energy 2001;68(2):173–85.
[6] Sözen A, Altparmak D, Usta H. Development and testing of a prototype of absorption heat pump system operated by solar energy. Appl Therm Eng 2002;22(16):1847–59.
[7] Kim D, Infante Ferreira C. Solar refrigeration options – a state-of-the-art review. Int J Refrig 2008;31(1):3–15.
[8] Yuksel YE, Ozturk M, Dincer I. Thermodynamic performance assessment of a novel environmentally-benign solar energy based integrated system. Energy Convers Manage 2016;119:109–20.
[9] Zheng D, Dong L, Huang W, Wu X, Nie N. A review of imidazolium ionic liquids research and development towards working pair of absorption cycle. Renew Sustain Energy Rev 2014;37:47–68.
[10] Nowaczyk U, Steimle F. Thermophysical properties of new working fluid systems for absorption processes. Int J Refrig 1992;15(1):10–5.
[11] Ameel TA, Gee KG, Wood BD. Performance predictions of alternative, low cost absorbents for open cycle absorption solar cooling. Sol Energy 1995;54(2):65–73.
[12] Donate M, Rodriguez L, Lucas AD, Rodríguez JF. Thermodynamic evaluation of new absorbent mixtures of lithium bromide and organic salts for absorption refrigeration machines. Int J Refrig 2006;29(1):30–5.
[13] Karamangil MI, Coskun S, Kaynakli O, Yamankaradeniz N. A simulation study of performance evaluation of single-stage absorption refrigeration system using conventional working fluids and alternatives. Renew Sustain Energy Rev 2010;14(7):1969–78.
[14] Sun J, Fu L, Zhang S. A review of working fluids of absorption cycles. Renew Sustain Energy Rev 2012;16(4):1899–906.
[15] Dong L, Zheng D, Nie N, Li Y. Performance prediction of absorption refrigeration cycle based on the measurements of vapor pressure and heat capacity of H_2O + [DMIM]DMP system. Appl Energy 2012;98:326–32.
[16] Abumandour E-S, Mutelet F, Alonso D. Performance of an absorption heat transformer using new working binary systems composed of {ionic liquid and water}. Appl Therm Eng 2016;94:579–89.
[17] Chen W, Liang S. Thermodynamic analysis of absorption heat transformers using [mmim]DMP/H_2O and [mmim]DMP/CH_3OH as working fluids. Appl Therm Eng 2016;99:846–56.
[18] Shiflett MB, Yokozeki A. Absorption cycle utilizing ionic liquid as working fluid. US2006/0197053 A1; 2006a.
[19] Ayou DS, Currás MR, Salavera D, García J, Bruno JC, Coronas A. Performance analysis of absorption heat transformer cycles using ionic liquids based on imidazolium cation as absorbents with 2,2,2-trifluoroethanol as refrigerant. Energy Convers Manage 2014;84:512–23.
[20] Cai W, Sen M, Paolucci S. Dynamic modeling of an absorption refrigeration system using ionic liquids. Proceedings of the ASME 2007 International Mechanical Engineering Congress and Exposition. Seattle: ASME; 2007. p. 227–36.
[21] Yokozeki A, Shiflett MB. Ammonia solubilities in room-temperature ionic liquids. Industr Eng Chem Res 2007;46(5):1605–10.
[22] Yokozeki A, Shiflett MB. Vapor-liquid equilibria of ammonia + ionic liquid mixtures. Appl Energy 2007;84(12):1258–73.
[23] Kotenko, O., 2012. Potential Analysis of Alternative Absorption Heat Pumping Processes with Special Emphasis on Sodium Hydroxide as Additive [Ph.D. thesis]. Graz University of Technology.
[24] Chen W, Liang S, Guo Y, Gui X, Tang D. Investigation on vapor-liquid equilibria for binary systems of metal ion-containing ionic liquid [bmim]Zn_2Cl_5/NH_3 by experiment and modified UNIFAC model. Fluid Phase Equilib 2013;360:1–6.
[25] Chen W, Liang S, Guo Y, Tang D. Thermodynamic analysis of an absorption system using [bmim]Zn_2Cl_5/NH_3 as the working pair. Energy Convers Manage 2014;85:13–9.
[26] Ruiz E, Ferro VR, De Riva J, Moreno D, Palomar J. Evaluation of ionic liquids as absorbents for ammonia absorption refrigeration cycles using COSMO-based process simulations. Appl Energy 2014;123:281–91.
[27] Shiflett MB, Yokozeki A. Solubility and diffusivity of hydrofluorocarbons in room-temperature ionic liquids. AIChE J 2006;52(3):1205–19.
[28] Kim YJ, Kim S, Joshi YK, Fedorov AG, Kohl PA. Thermodynamic analysis of an absorption refrigeration system with ionic-liquid/refrigerant mixture as a working fluid. Energy 2012;44(1):1005–16.
[29] Harrison BK, Seaton WH. Solution to missing group problem for estimation of ideal gas heat capacities. Industr Eng Chem Res 1988;27(8):1536–40.
[30] Radspieler M, Schweigler C. Experimental investigation of ionic liquid Emim $EtSO_4$ as solvent in a single-effect cycle with adiabatic absorption and desorption. In: Proceedings of the international sorption heat pump conference (ISHPC11). IIR/AICARR, Padua; 2011, p. 125–34.
[31] Schneider M-C, Schneider R, Zehnacker O, Buchin O, Cudok F, Kühn A, et al. Ionic liquids: new-high performance working fluids for absorption chillers and heat pumps. In: Proceedings of the International Sorption Heat Pump Conference (ISHPC11). IIR/AICARR, Padua; 2011, p. 95–106.
[32] Wasserscheid P, Seiler M. Leveraging gigawatt potentials by smart heat-pump technologies using ionic liquids. ChemSusChem 2011;4(4):459–63.
[33] Kim S, Kim YJ, Joshi YK, Fedorov AG, Kohl PA. Absorption heat pump/refrigeration system utilizing ionic liquid and hydrofluorocarbon refrigerants. J Electron Packag 2012;134(3):15–30.
[34] Meyer T, Kühn R, Ricart C, Zegenhagen T, Ziegler F. Simulation of an absorption refrigerator working with ionic liquids and natural refrigerants. In: Proceedings of the 24th IIR international congress of refrigeration. Yokohama; 2015, paper ID 859.
[35] Ariyadi HM, Coronas A. Absorption capacity of ammonia into ionic liquids for absorption refrigeration applications. J Phys: Conf Ser 2016;745:032105.
[36] Wadekar VV. Ionic liquids as heat transfer fluids – an assessment using industrial exchanger geometries. Appl Therm Eng 2017;111:1581–7.
[37] Boman DB, Hoysall DC, Staedter MA, Goyal A, Ponkala MJ, Garimella S. A method for comparison of absorption heat pump working pairs. Int J Refrig 2017;77:149–75.
[38] Chugh D, Gluesenkamp K, Abdelaziz O, Moghaddam S. Ionic liquid-based hybrid absorption cycle for water heating, dehumidification, and cooling. Appl Energy 2017;202:746–54.
[39] Kiss AA, Infante Ferreira CA. Heat pumps in chemical process industry. CRC Press; 2016.
[40] Lemmon EW, Huber ML, McLinden MO. NIST reference fluid thermodynamic and transport properties-REFPROP; 2013.
[41] Yokozeki A, Shiflett MB. Water solubility in ionic liquids and application to absorption cycles. Industr Eng Chem Res 2010;49(19):9496–503.
[42] Valderrama JO, Robles PA. Critical properties, normal boiling temperatures, and acentric factors of fifty ionic liquids. Industr Eng Chem Res 2007;46(4):1338–44.
[43] Sun G, Zheng D, Huang W, Dong L. The measurement of ammonia solubility in the ionic liquid 1, 3-dimethylimidazolium dimethylphosphate ([Dmim]DMP) (in Chinese). J Beijing Univ Chem Technol. (Nat Sci Ed) 2012;39(4):17–21.
[44] Li G, Zhou Q, Zhang X, LeiWang, Zhang S, Li J. Solubilities of ammonia in basic imidazolium ionic liquids. Fluid Phase Equilib 2010;297(1):34–9.
[45] Sassen CL, van Kwartel RAC, van Der Kooi HJ, de Swaan Arons J. Vapor-liquid equilibria for the system ammonia + water up to the critical region. J Chem Eng Data 1990;35:140–4.
[46] Paulechka YU. Heat capacity of room-temperature ionic liquids: a critical review. J Phys Chem Ref Data 2010;39(3):033108.
[47] He Z, Zhao Z, Zhang X, Feng H. Thermodynamic properties of new heat pump working pairs: 1,3-Dimethylimidazolium dimethylphosphate and water, ethanol and methanol. Fluid Phase Equilib 2010;298(1):83–91.
[48] Yu YH, Soriano AN, Li MH. Heat capacities and electrical conductivities of 1-ethyl-3-methylimidazolium-based ionic liquids. J Chem Thermodyn 2009;41(1):103–8.
[49] Waliszewski D. Heat capacities of the mixtures of ionic liquids with methanol at temperatures from 283. 15 K to 323.15 K. J Chem Thermodyn 2008;40(2):203–7.
[50] Paulechka YU, Blokhin AV, Kabo GJ. Evaluation of thermodynamic properties for non-crystallizable ionic liquids. Thermochim Acta 2015;604:122–8.
[51] Kabo GJ, Blokhin AV, Paulechka YU, Kabo AG, Shymanovich MP, Magee JW. Thermodynamic properties of 1-butyl-3-methylimidazolium Hexafluorophosphate in the condensed state. J Chem Eng Data 2004;49(3):453–61.
[52] Paulechka YU, Blokhin AV, Kabo GJ, Strechan AA. Thermodynamic properties and polymorphism of 1-alkyl-3-methylimidazolium bis(triflamides). J Chem Thermodyn 2007;39(6):866–77.
[53] Navarro P, Larriba M, Rojo E, García J, Rodríguez F. Thermal properties of cyano-based ionic liquids. J Chem Eng Data 2013;58(8):2187–93.
[54] Zhang ZB, Zhou Q, Lu XM, Qiao CZ, Zhang SJ. Densities and viscosities of binary mixtures containing 1,3-Dimethylimidazolium Dimethylphosphate and alcohols. J Chem Eng Data 2014;59(8):2377–88.
[55] Salgado J, Regueira T, Lugo L, Vijande J, Fernández J, García J. Density and viscosity of three (2,2,2-trifluoroethanol + 1-butyl-3-methylimidazolium) ionic

liquid binary systems. J Chem Thermodyn 2014;70:101–10.
[56] Hofmann A, Migeot M, Hanemann T. Investigation of binary mixtures containing 1-Ethyl-3-methylimidazolium Bis(trifluoromethanesulfonyl)azanide and Ethylene Carbonate. J Chem Eng Data 2016;61(1):114–23.
[57] Freire MG, Teles ARR, Rocha MAA, Schröder B, Neves CMSS, Carvalho PJ, et al. Thermophysical characterization of ionic liquids able to dissolve biomass. J Chem Eng Data 2011;56(12):4813–22.
[58] Wimby JM, Berntsson TS. Viscosity and density of aqueous solutions of lithium bromide, lithium chloride, zinc bromide, calcium chloride and lithium nitrate. 1. Single salt solutions. J Chem Eng Data 1994;39(1):68–72.
[59] Römer J, Jong M. Warmte- en koedevraagpatronen in de utiliteitsbouw (in Dutch). Tech. rep., ECN; 1999.
[60] Yan Y-Y, Lio H-C, Lin T-F. Condensation heat transfer and pressure drop of refrigerant R-134a in a plate heat exchanger. Int J Heat Mass Transfer 1999;42(6):993–1006.
[61] Khan MS, Khan TS, Chyu M-C, Ayub ZH. Experimental investigation of evaporation heat transfer and pressure drop of ammonia in a 30° chevron plate heat exchanger. Int J Refrig 2012;35(6):1757–65.
[62] Thonon B, Bontemps A. Condensation of pure and mixture of hydrocarbons in a compact heat exchanger: experiments and modelling. Heat Transfer Eng 2002;23(6):3–17.
[63] Tenney CM, Massel M, Mayes JM, Sen M, Brennecke JF, Maginn EJ. A computational and experimental study of the heat transfer properties of nine different ionic liquids. J Chem Eng Data 2014;59(2):391–9.
[64] DACE, 2015. DACE (Dutch Association of Cost Engineers) price booklet November 2015, 31st ed., The Hague.
[65] Eurostat. Energy price statistics. <http://ec.europa.eu/eurostat/statistics-explained/index.php/Energy_price_statistics>; 2016.
[66] Chen L, Sharifzadeh M, Mac Dowell N, Welton T, Shah N, Hallett JP. Inexpensive ionic liquids: [HSO_4]-based solvent production at bulk scale. Green Chem 2014;16(6):3098.
[67] Honeywell UOP. Honeywell UOP Introduces Ionic Liquids Alkylation Technology. URL <https://www.uop.com/?press_release=honeywell-uop-introduces-ionic-liquids>; 2016.
[68] Earle MJ, Esperança JM, Gilea MA, Canongia Lopes JN, Rebelo LP, Magee JW, et al. The distillation and volatility of ionic liquids. Nature 2006;439(7078):831–4.